Polymer Testing 148 (2025) 108835

Contents lists available at ScienceDirect

Polymer Testing

journal homepage: www.elsevier.com/locate/polytest

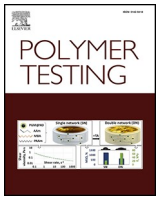

Dynamic mechanical performance of a pre-compressed high damping rubber-based elastomer for vibration damping systems

Jia-Xuan He [a], Zhao-Dong Xu [a,*], Zhong-Wei Hu [a], Teng Ge [b], Qiang-Qiang Li [c], Yao-Rong Dong [d], Gabriele Milani [e,**]

[a] China-Pakistan Belt and Road Joint Laboratory on Smart Disaster Prevention of Major Infrastructures, Southeast University, Nanjing, 210096, China
[b] School of Civil and Transportation Engineering, Hohai University, Nanjing, 210024, China
[c] School of Civil Engineering and Architecture, Xi'an University of Technology, Xi'an, 710048, China
[d] School of Civil Engineering, Xi'an University of Architecture and Technology, Xi'an, 710055, China
[e] Department of Architecture, Built Environment and Construction Engineering, Politecnico di Milano, Milan, 20133, Italy

ARTICLE INFO

Keywords:
High damping engineering elastomer
Dynamic mechanical performance
Energy dissipation mechanism
Pre-compression effect
Temperature dependence

ABSTRACT

Vibration damping elastomers often operate under preload engineering scenarios, which demand enhanced dynamic performance in coupled service environments. This study investigated the mechanical behavior of a high damping rubber-based elastomer under pre-compression, cyclic loading, and thermal conditions. The elastomer is based on carboxylated nitrile-butadiene rubber (XNBR) as the matrix and is modified through nanofiller reinforcement and sacrificial bonds. This modification effectively overcomes the conventional conflict between damping efficient and mechanical strength. The mechanical behaviors of pre-compressed elastomers were comprehensively evaluated using quasi-static compression test, low-to-medium frequency cyclic test, and temperature-controlled cyclic test. These tests were conducted under varying frequencies, pre-compressions, amplitudes, and temperatures, which considered coupled service conditions. Test results demonstrated that pre-compression allowed the operational region of cyclic loading to shift along the hyperelastic stress-strain curve, providing higher stiffness and resistance in service. The high damping rubber-based elastomer significantly improved mechanical properties with increasing frequency from 0.1 Hz to 20.0 Hz. Within general ambient temperatures, low temperatures amplified modulus and energy dissipation. Amplitude-driven softening slightly reduced the equivalent modulus but markedly amplified hysteretic energy dissipation, especially under high pre-compression. The high damping rubber-based elastomer exhibited high damping performance over a wide frequency band (0.1–20.0 Hz) and a wide temperature range (10.0–40.0 °C). Appropriate amplitude and well-designed pre-compression dramatically enhanced energy dissipation with suitable bearing capacity. On a microscopic scale, the synergistic effects of polymer chain mobility, filler-matrix interaction, and hydrogen bond dynamic equilibrium explain the compressive behavior and dynamic energy dissipation mechanisms. These findings established a universal framework for designing the high damping rubber-based elastomer with tailored compressive and damping performance, enabling its application in diverse vibration control scenarios requiring precision and adaptability.

1. Introduction

Vibration damping elastomers constitute indispensable components in traditional engineering fields owing to their capacity for reversible deformation and energy dissipation under cyclic loads [1–7]. The applications of vibration damping elastomers span a wide range, from seismic mitigation and isolation in civil infrastructure to precision vibration control in aerospace and automotive industries [8–13,58]. A fundamental challenge in conventional elastomers lies in the conflict between damping capacity and mechanical resilience. Enhanced damping capacity typically compromises load-bearing capacity and recoverability, while improvements in mechanical resilience generally reduce energy dissipation efficiency. Current engineering solutions strategically utilize the inherent nonlinear stress-strain behavior of most

* Corresponding author.
** Corresponding author.
E-mail addresses: zhdxu@163.com (Z.-D. Xu), gabriele.milani@polimi.it (G. Milani).

https://doi.org/10.1016/j.polymertesting.2025.108835
Received 11 March 2025; Received in revised form 14 April 2025; Accepted 1 May 2025
Available online 1 May 2025

elastomers as a critical design advantage. In civil engineering applications, rubber bumpers and advanced polymeric absorbers are incorporated between adjacent buildings or bridge segments, where their nonlinear elastic response effectively mitigates collision-induced impact pulses [14]. For damping device optimization, pre-compressed rubber cylinders have demonstrated excellent results in achieving a balance between self-centering capability and energy dissipation through controlled nonlinear deformation [15,16,57]. Furthermore, thick rubber bearing systems employ nonlinear stiffness for superstructure support, while reducing subway-induced micro-vibrations by fully utilizing the damping properties of elastomers [17]. In these applications, vibration damping elastomers are required to offer high damping efficiency for energy dissipation, sufficient structural stiffness for load-bearing, and exceptional cyclic repeatability to prevent performance degradation phenomena such as ratcheting effects or irreversible microstructural damage [18–20]. Therefore, a clear requirement for vibration damping elastomers emerges, which is simultaneously achieve reliable load-bearing capacity under heavy loads and excellent vibration damping capacity during dynamic excitation events.

Conventional rubber-based elastomers dissipate energy through molecular chain friction within polymer networks, which generally leads to irreversible network degradation and a narrow operational temperature window [21–23]. In practical service environments, the effective damping temperature range of 20–30 °C falls below ambient conditions, while simultaneously efficient energy dissipation is required over a wide frequency band (e.g., 0.1–20.0 Hz or higher) [24]. These performance limitations are addressed through elastomer reinforcement strategies, such as nanofiller reinforcement and sacrificial bonds.

The incorporation of nanofillers offers a promising strategy to enhance both the mechanical and functional performances of rubber-based elastomers, expanding their application potential [25–27]. Nanofiller addition reduces the free volume within the polymer matrix, increases stiffness, and establishes intense filler-matrix interactions. These changes lead to the formation of nanocomposite elastomers with exceptional properties even at relatively low filler loadings. Recent studies have demonstrated that incorporating nanofillers into carboxylated nitrile-butadiene rubber (XNBR) significantly enhances its mechanical performance, thermal stability, and damping properties [28–31]. These advancements make the XNBR-based nanocomposites particularly attractive for advanced engineering applications that demand high performance. On the other hand, sacrificial bonding mechanisms have demonstrated remarkable potential for developing advanced high-performance elastomers [32,33]. This approach simultaneously improves the strength and toughness of elastomers. It enables the design of durable elastomeric materials without necessitating complex chemical modifications. The sacrificial bonds function as reversible energy dissipation that protects the primary polymer network from catastrophic failure during cyclic loading events. The preferential rupture and dynamic features of sacrificial bonds prevent local stress concentration on a molecular level throughout the network. This facilitates the slippage and orientation of polymer chains when deformation is applied.

Importantly, the mechanical performance and internal microscopic mechanism of these developed elastomers need to be evaluated under simulated loading scenarios approaching reality. Gong [34] examined the time-varying law and mechanism of compression performance under arbitrary pre-compression strain, simulating the long-term performance of ethylene propylene diene monomer under complex compression. Vatandoost [35] studied the pre-strain dependence of the dynamic properties of magnetorheological elastomers under compression, correlating it to the volume fraction of particles. Mistry [36] incorporated the anisotropic ordering of liquid crystals into elastic polymer networks to produce liquid crystal elastomers, introducing and controlling the nature of buckling responses during compression. Persson [37] explored the temperature dependence of a thermoplastic vulcanizate elastomer under cyclic compression, which was influenced by the presence of multiple phases. While these studies have been conducted under service conditions tailored to specific engineering applications, research on vibration damping elastomers is often limited to simplified scenarios, such as static and dynamic tests in shear or compression. These tests reveal frequency-, amplitude-, and temperature-dependent behaviors of vibration damping elastomers in shear or compression, but fail to capture the full complexity of real applications. Some investigations have studied vibration damping devices under complex operating scenarios. However, technical limitations still restrict these evaluations, especially when it comes to precise temperature control for large-scale specimens.

Vibration damping elastomers require rigorous evaluation under coupled service conditions, which are simultaneously withstand high pre-strain, cyclic loading, and thermal variations. The interaction between pre-compression, dynamic loads, and variable ambient temperatures can significantly influence both stiffness and energy dissipation mechanisms, especially considering the nonlinear effects under pre-compression. Consequently, understanding these complex interdependencies is essential for developing predictive models that accurately reflect the behavior and reliability of damping elastomers. In addition, further investigation into the microscopic energy dissipation mechanisms under these coupled conditions is necessary to optimize performance and establish design guidelines.

In our previous work, a novel high damping rubber-based elastomer was developed by integrating nanofiller reinforcement with sacrificial bonding mechanism [44]. This engineered elastomer exhibits an effective damping temperature range of −20.0 to 40.0 °C and maintains excellent damping performance across a frequency range of 0.001–10000 Hz [38–41]. Earlier studies have also confirmed that this elastomer demonstrates outstanding energy dissipation capacity and high recoverability under cyclic compressions spanning small to large deformations [42]. Building on these findings, the pre-compression performance of the high damping rubber-based elastomer is further investigated in vibration damping system. This study begins by detailing the design, preparation, and basic material properties of the high damping rubber-based elastomer. Test protocols were established to evaluate its mechanical behavior under coupled pre-compression, cyclic loading, and thermal conditions. Macroscopic nonlinear stiffness and damping performance were correlated with underlying microscopic mechanisms such as chain mobility, filler-matrix interfacial friction, and hydrogen bond dynamics. The results combine macroscopic performance indicators, microscopic mechanism analysis, and consider the coupling effects of pre-compression, frequency, amplitude, and temperature, providing a solid reference for improving the design of engineering elastomers and vibration damping systems.

2. Experimental

2.1. Material

The high damping rubber-based elastomer investigated in this study was specifically engineered for vibration damping applications. The elastomer mainly consisted of XNBR blended with organic polar small molecules (AO-80 hindered phenol), nanofiller (carbon black), and co-adjuvants (zinc oxide). The effective particle size of the carbon black is 150 nm, and the specific surface area is greater than 700 m^2/g. Detailed information on the materials can be found in our previous work [43]. XNBR, a modified nitrile rubber containing carboxyl groups in its polymer chains, is a noncrystalline elastomer with limited unsaturated carbon chains. Unlike crystallizable rubbers exhibiting strong self-reinforcement, XNBR demonstrates inherent weak reinforcement [44].

To overcome this limitation, nanofillers and sacrificial bonds were implemented to achieve the reinforcement of XNBR. In this composite system, carbon black fillers establish percolation networks that restrict polymer chain mobility and induce interfacial friction during cyclic

deformation. Hydrogen bonds were selected to serve as sacrificial bonding due to chemical compatibility, dynamic reversibility, and temperature responsiveness [45,46]. Hydrogen bonding forms between polar nitrile groups (-C ≡ N) in XNBR and hydroxyl groups (-OH) from organic small molecules, as illustrated in Fig. 1.

At the microscopic level, chemical crosslinks, hydrogen bonds, and fillers play unique but complementary roles in constructing the polymer network, together forming a multi-level, integrated network structure. First, chemical crosslinking reactions create strong covalent bonds between molecular chains, which establish the fundamental elastic network. This crosslinked network primarily provides the main structural stability and mechanical strength. Second, fillers, such as carbon black, act as additional physical crosslinks and reinforcing aggregates, stabilizing the polymer network and limiting the local chain motion. As a result, the bearing capacity of the polymer is enhanced, the risk of damage is reduced, and energy dissipation is improved. Third, building on the fundamental molecular chain network, polar groups on free chains interact with organic polar small molecules to form hydrogen bonds, resulting in a dynamic secondary network. The reversible nature and high-density distribution of these bonds allow them to break and reform promptly in response to external disturbances (e.g., mechanical deformations or temperature changes). This behavior promotes effective energy absorption and dissipation. The dynamic characteristic leads to high damping at room temperature and also provides the material with dynamic reversibility. In short, the system achieves a balance between stability and dynamic response on the molecular level. With the assistance of fillers and hydrogen bonds, it effectively improves the mechanical strength, durability, and damping performance on a macroscopic scale.

2.2. Preparation

The manufacturing process commenced with the plasticization of XNBR raw material in a closed internal mixer, where mechanical shearing and thermal softening transformed the rubber into a malleable state. Following plasticization, compounding additives (AO-80, zinc oxide, stearic acid, carbon black, accelerating agent, antioxidant, and sulfur) were sequentially incorporated through a standardized mixing protocol. The rubber compound was thoroughly rubbed and blended using rotors and heating jackets to produce a homogeneous mass. It was subsequently processed on a two-roll rubber mill for open mixing and finally rolled into sheets. Curing time were measured at 160 °C on the no-rotor rheometer [44]. The prepared rubber compound was filled into molds and subjected to heat and pressure in the vulcanizing machine at 160 °C and 15 MPa for 50 min. This ensured sufficient vulcanization at the core of the cylindrical specimen, in accordance with the production indications provided in Refs. [47–49]. The finished, vulcanized product is illustrated in Fig. 5. The compound underwent intensive blending using counter-rotating rotors for 8–10 min until uniform filler distribution. Subsequent open mixing on a two-roll mill produced 3 mm-thick sheets with directional homogeneity. The prepared rubber compound was filled into molds and subjected to heat and pressure in the vulcanizing machine, resulting in finished products.

The microscopic characteristics of the elastomer were observed by scanning electron microscopy, as illustrated in Fig. 2. At the 500 nm resolution scale, fillers demonstrated a homogeneous dispersion within the polymer matrix, with carbon black agglomerations in the local area. The fillers maintained robust interfacial adhesion to the matrix without discernible debonding or crack initiation. The surface topography displayed roughness accompanied by protrusions, enhancing the specific surface area. A cross-sectional examination of cryogenically fractured surfaces at 50 nm resolution revealed a densely packed microstructure interspersed with nanoscale cavities. These cavities originated from the fallout of agglomerated carbon black. The absence of large defects or interfacial delamination corroborated the effective stress transfer capability at filler-matrix interfaces.

2.3. Basic material properties

The basic material properties of the high damping rubber-based material were characterized through standardized testing protocols. The specific experimental procedures and results were summarized as follows, and the measured results were list in Table 1 and depicted in Figs. 3 and 4. Considering application scenarios for vibration damping systems in civil engineering, the test conditions were deliberately chosen to reflect the operational environment of these systems.

Shore A hardness measurements were conducted in accordance with GB/T 531.1–2008 and ASTM D2240 using a calibrated Shore hardness durometer. Five replicate tests were performed on specimens with lateral dimensions ensuring a minimum edge distance of 12 mm.

Dumbbell-shaped specimens (Type II per GB/T 528–2009) with gauge section dimensions of 4 mm (width) × 2 mm (thickness) were tested under uniaxial tension at a controlled temperature of 13 ± 2 °C and a crosshead speed of 500 mm/min. These tests were performed on a

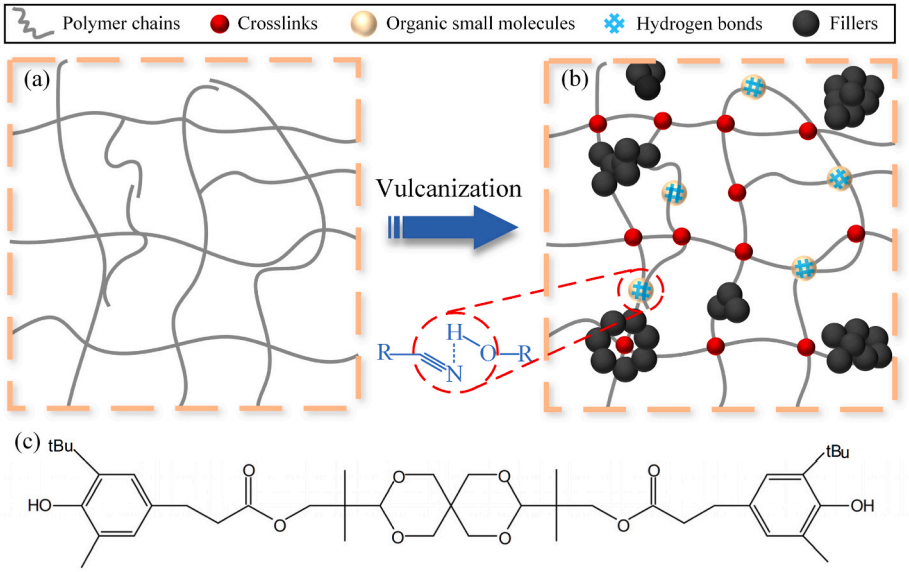

Fig. 1. Microstructure: (a) raw XNBR, (b) high damping rubber-based elastomer, and (c) AO-80.

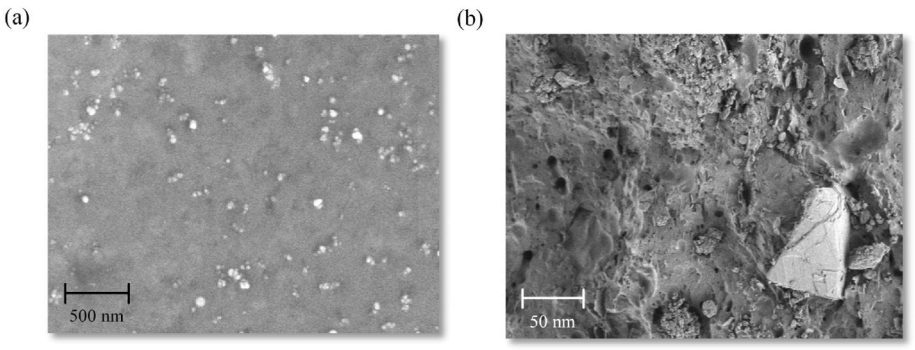

Fig. 2. Scanning electron microscope image.

Table 1
Basic material properties.

Material properties	Value
Shore A hardness (HA)	65
Tensile strength (MPa)	7.896
Elongation at break (%)	438.7
Residual stress ratio (%)	53.0
Storage modulus (MPa)	1.16
Loss factor	1.69

universal tensile testing machine. To ensure accurate tracking of deformation within the critical zone, local strains were directly measured using an extensometer attached to the gauge section of these specimens during the tensile tests. Tensile strength σ_t and elongation at break e_b were calculated using:

$$\sigma_t = \frac{P_{max}}{wt} \tag{1}$$

$$e_b = \frac{L_b - L_0}{L_0} \times 100\% \tag{2}$$

where P_{max}, w, t, L_b, and L_0 represent the peak force, initial width, initial thickness, fractured length, and original gauge length, respectively.

Stress relaxation behavior was investigated using a universal tensile testing machine. Specimens were stretched to 50 % nominal strain in accordance with GB/T 9871-2008. The deformation was then maintained for 300 s under isothermal conditions at 13 ± 2 °C. The residual stress ratio ξ_r is defined as the percentage of retained stress after relaxation relative to the initial stress, was quantified as:

$$\xi_r = \frac{\sigma_s}{\sigma_0} \times 100\% \tag{3}$$

where σ_s and σ_0 denote the stress at time $t = 300$ s and the initial stress, respectively.

The double shear test was used to determine the storage modulus G' and loss factor η of high damping rubber-based elastomers. Double cuboid specimens with 10 mm thickness and 60 × 50 mm^2 shear area were bonded via vulcanization between rigid steel plates, ensuring uniform shear strain. Tests were performed on a $w + b$ dynamic testing system. Specimens were subjected to harmonic displacement loading at a frequency of 0.5 Hz. The shear strain amplitudes were varied between 5 % and 50 %, with the nominal strain values defined by the displacement control of actuator. Each amplitude underwent five cycles, with the last three cycles averaged to compute G' and η.

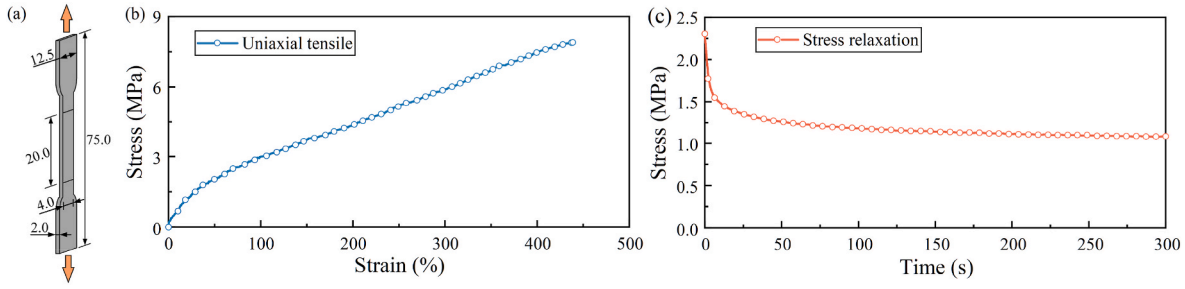

Fig. 3. (a) Tensile specimen geometry (unit: mm), (b) Uniaxial tensile curve, and (c) Tensile stress relaxation curve.

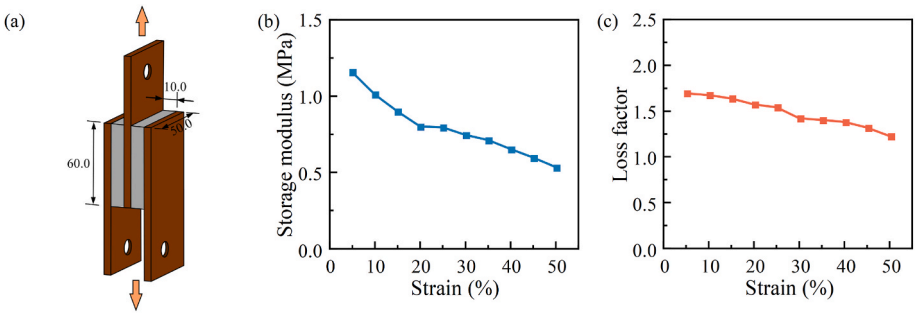

Fig. 4. (a) Double shear specimen geometry (unit: mm), (b) Storage modulus, and (c) Loss factor.

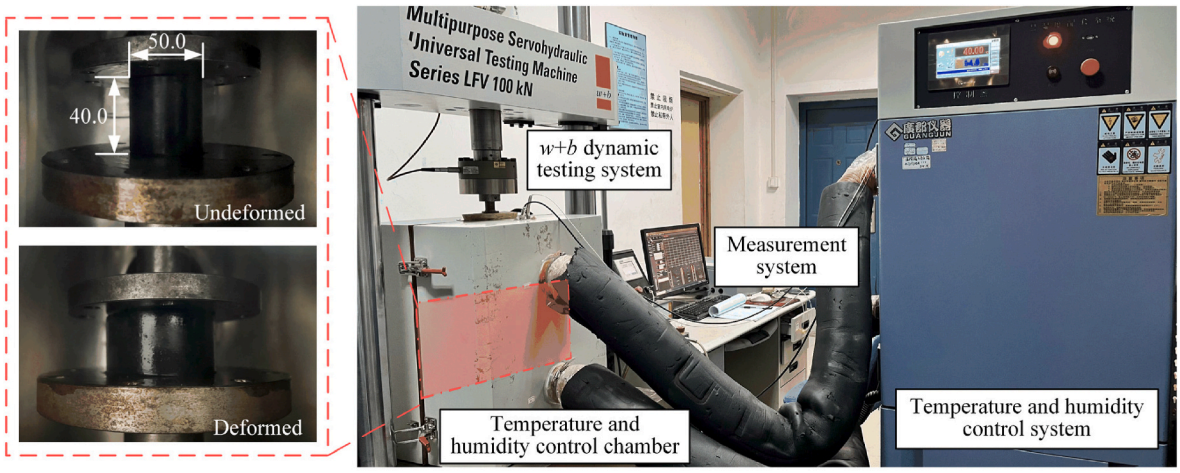

Fig. 5. Test setup and uniformly deformed specimen. (unit: mm).

The storage modulus and loss factor, which quantifies the elastic energy stored and energy dissipation efficiency, are defined as:

$$G' = \frac{F_1 h_v}{n_v A_v u_0} \tag{4}$$

$$\eta = \frac{F_2}{F_1} \tag{5}$$

where u_0 and F_1 are the maximum loading displacement and its corresponding damping force; F_2 is the damping force when the displacement is zero.

Environmental controls maintained a temperature of 13 ± 2 °C. System calibration, thermal drift correction, and five validation ensured repeatability.

2.4. Pre-compressed mechanical testing

Elastomers in vibration damping systems usually exist in the pre-loaded state, and the above basic material properties fails to adequately represent the service performance. Pre-compressed mechanical testing was performed on a $w + b$ dynamic testing system with a maximum force capacity of 100 kN and a ±60 mm stroke range, as shown in Fig. 5. The tests were conducted under displacement-controlled conditions. The test procedure complied ASTM D5992-96, GB/T 7757-2009/ISO 7743:2007, and HG/T 3843-2008. The specimens used were solid circular cylindrical samples measuring 50 ± 0.5 mm in diameter, and 40 ± 0.5 mm in height. Dimensional verifications of mass, height, diameter, hole diameter, and area were conducted to minimize experimental errors, and deviations remained below 1 %. The loading conditions are shown list in Table 2.

Specimens were carefully centered on high-strength steel platens (on the vertical axis of the loading actuator), and both the upper and lower surfaces were lubricated with sufficient dimethyl silicone oil to reduce friction and ensure relatively uniform compression. Environmental conditions were regulated via an integrated temperature and humidity control system. Force-displacement data were acquired through embedded sensors in the dynamic testing system, while environmental parameters were monitored separately.

2.4.1. Quasi-static uniaxial compression testing

Given the inherent viscoelastic nature of the rubber-based material, quasi-static testing at a low loading rate (2.0 mm/min) was implemented to characterize its elastic properties while minimizing time-dependent effects. Uniaxial compression was performed under ambient conditions (23 ± 2 °C) until achieving a maximum displacement of 10.0 mm, corresponding to an engineering strain of 25 % (nominal strain rate maintained below 10^{-3} s^{-1}).

2.4.2. Low-to-medium frequency cyclic compression testing

The specimens underwent systematic pre-compression protocols to establish baseline stress states before dynamic testing. Using displacement-controlled loading at 2.0 mm/min, three pre-compression levels (3.0, 5.0, and 7.0 mm) were sequentially applied to achieve mechanical equilibrium. This was followed by sinusoidal cyclic loading with corresponding amplitudes (1.0, 2.0, and 3.0 mm, respectively). Frequency sweeps from 0.1 Hz to the system-limited maximum of 20.0 Hz were conducted at ambient temperature (23 ± 2 °C). Five complete cycles were recorded for each frequency-amplitude combination. The experimental design simulated operational preloading conditions in vibration control applications, such as seismic isolation bearings, railway dampers, and automotive suspensions. This approach enabled precise quantification of energy dissipation characteristics across low-to-medium frequency domains (0.1–20.0 Hz).

Table 2
Loading cases.

Test	Experimental variable			
Quasi-static compression test	Deformation (mm) 10.0	Loading rate (mm/min) 2.0		
Low-to-medium frequency dynamic cyclic test	Amplitude (mm) 1.0 2.0 3.0	Pre-compression (mm) 3.0, 5.0, 7.0 5.0, 7.0 7.0	Frequency (Hz) 0.1, 0.5, 1.0, 3.0, 5.0, 10.0, 15.0, 20.0	
Temperature-controlled dynamic cyclic test	Amplitude (mm) 1.0 2.0 3.0	Pre-compression (mm) 3.0, 5.0, 7.0, 10.0 5.0, 7.0, 10.0 7.0, 10.0	Frequency (Hz) 0.1, 0.5, 1.0, 3.0	Temperature (°C) 10.0, 20.0, 30.0, 40.0

2.4.3. Temperature-controlled cyclic compression testing

In temperature-controlled dynamic cyclic tests, the chosen experimental variables (frequency, amplitude, pre-compression, and temperature) were designed to simulate both seismic characteristics and practical operating conditions of rubber-based damping devices. Pre-compression levels (3.0, 5.0, 7.0, and 10.0 mm) were coupled with displacement amplitudes through progressive pairing:

- 1.0 mm amplitude for all pre-compression levels
- 2.0 mm amplitude for ≥5.0 mm pre-compression
- 3.0 mm amplitude for ≥7.0 mm pre-compression

Sinusoidal loading was applied across seven loading frequencies of 0.1, 0.2, 0.3, 0.5, 1.0, 2.0, and 3.0 Hz for five complete cycles per variable combination. The environmental conditions were maintained at four discrete temperature setpoints (10.0, 20.0, 30.0, and 40.0 °C) with relative humidity regulated between 30 and 60 %. To ensure the accuracy and reliability of the temperature-controlled test results, a 30-min thermal equilibration period preceded each test sequence to obtain specimen temperature homogeneity (±1.0 °C).

In summary, these tests allowed for a comprehensive evaluation of the mechanical behavior of the material under varying environmental and operational conditions. The loading cases of mechanical tests are listed in Table 1. To clearly indicate and label each loading case, a shorthand notation is used. In this notation, QST denotes the quasi-static compression test, D represents the loading amplitude (mm), P specifies the pre-compression value (mm), F indicates the loading frequency (Hz), and T means the experimental temperature (°C). The loading cases of dynamic cyclic test are presented in the format D■P■F■T■, where ■ denotes the numerical value of the corresponding variables. This notation also serves to reference experimental datasets across variable combinations. For instance, the notation P10.0F1.0 refers to all test data acquired under the conditions of 10.0 mm pre-compression and 1.0 Hz loading frequency. The loading amplitude ranged from 1.0 to 3.0 mm, while the experimental temperature varied between 10.0 and 40.0 °C.

3. Results and discussion

3.1. Results of quasi-static compression testing

The stress-strain curve exhibited nonlinear behavior and progressive stiffness with increasing strain, demonstrating a clear progressive stress-strain phenomenon, as shown in Fig. 6 (a). The elastomers displayed hyperelasticity and recoverability under large deformations, returning immediately to the original state upon unloading.

For polymer materials, the microscopic molecular dynamics significantly influence the mechanical properties on the macroscopic scale, which can be explained by the changes in multi-level, integrated polymer networks under external forces [50–52]. Under continuous stress, many chain segments begin to move and orient themselves, leading to large deformations on the specimen. The movement and orientation of chain segments eventually result in the organized polymer network. The introduction of fillers into the system further restricts the freedom of chain segments through physical hindrance, thereby improving the stiffness and strength of the elastomers. Molecular conformations are changed through internal rotation while the energy remains constant, allowing the specimen to return to its initial state even subject to large deformations. In addition, the incorporation of hydrogen bonds, a weak and reversible dynamic interaction, facilitates a balance between deformability and stiffness in polymers. The addition of fillers and hydrogen bonds changes the path of energy storage and dissipation. By enhancing effective crosslink density, promoting elastic energy storage, and restricting chain segment motion, the energy storage mechanism of hydrogen-bonded and filled networks enables the elastomers to approach an ideal network under low and moderate strains. As a result, the elastomers exhibit an almost linear elastic mechanical response. When the deformation exceeds the hydrogen bond stability range and the binding strength of the filler-matrix interface, nonlinear effects gradually appear.

3.2. Results of low-to-medium frequency dynamic cyclic testing

To investigate the effect of initial pre-deformation, selected results were analyzed. Without accounting for the temperature influence, the preloading paths were expected to align with the equilibrium curve, as drawn in Fig. 6 (a). The preloading paths of these force-displacement curves before cyclic loading matched the hyperelastic curve obtained from the quasi-static compression test. This indicates that pre-compression, frequency, and amplitude have no influence on the static preloading path. Stress-strain curves with pre-deformation under different pre-compressions, frequencies, and amplitudes were compared, as illustrated in Fig. 6(b)–(d).

A substantial hysteresis of the strain response was observed during unloading from the peak stress, indicating the inherent viscous nature of the rubber-based elastomers. As the number of cycles increased, the area of the force-displacement hysteresis loop gradually diminished. This

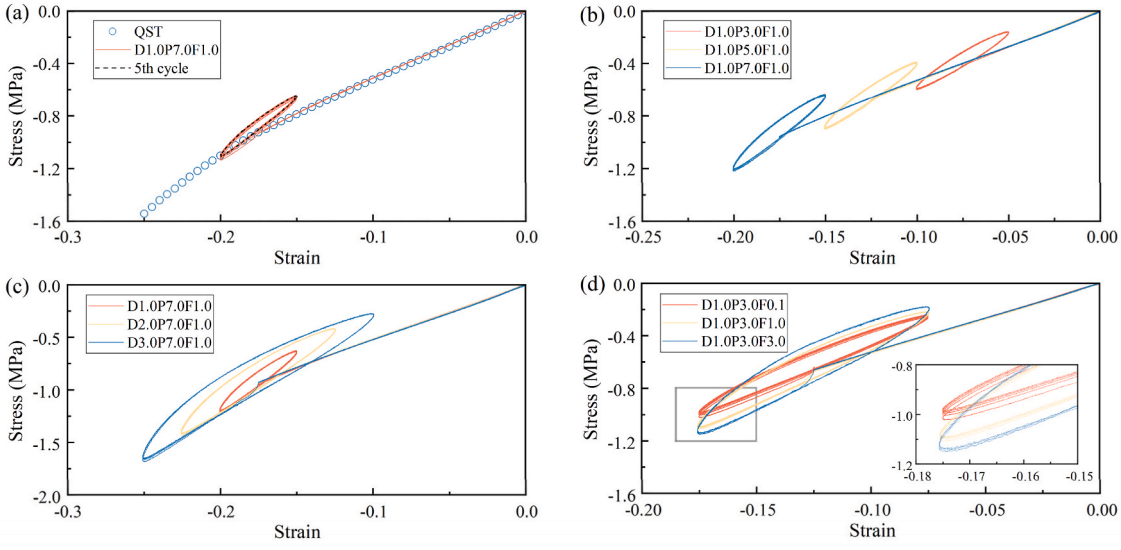

Fig. 6. Compassion of stress-strain curves with preload path and Mullins effect.

effect was especially pronounced after the first cycle, eventually reaching a stable state. The maximum force in the second cycle was noticeably lower than that in the first cycle, suggesting that the Mullins effect performs a crucial role at the first loading. The Mullins effect refers to the stress-softening phenomenon observed in elastomers during the initial loading cycles [53]. Continuous stress softening also occurred during subsequent cyclic loading. However, the degree of stress softening was less than that observed in the Mullins effect, and it is attributed to a fatigue effect. Compared to the results of previous unpre-compressed tests [42], the Mullins effect and fatigue effect subjected to pre-compression were not apparent and can be ignored in subsequent analysis.

Engineering applications of damping devices typically employ pre-compressed configurations, where energy dissipation capacity is evaluated using strain defined as the loading displacement normalized by the pre-compressed specimen height. Given the challenge of determining real-time contact area during deformation, stress calculations retained the original cross-sectional area before pre-compression. The stress-strain curves of the pre-compressed specimen after removing the pre-loading path and Mullins effect were presented in Fig. 7, in which the average curve of the last three (3rd, 4th, and 5th) cycles was used to identify definitive mechanical properties on a low-to-medium frequency band of 0.1 Hz–20.0 Hz.

Cyclic loading tests revealed progressive nonlinear viscoelastic behavior with increasing mechanical excitation. Elevated pre-compression increased material modulus and induced hysteresis loop distortion from ideal elliptical shapes. Concurrent increases in frequency and amplitude amplified nonlinear responses through loop inclination and inflation.

The mechanical performance indicators can be calculated by the following equations. These indicators include the equivalent modulus (defined as the slope of the virtual line connecting the initial loading point and maximum amplitude point), hysteretic energy (the area enclosed by hysteresis loops), and equivalent damping ratio (the relationship between energy consumption and elastic energy in one cycle).

The equivalent modulus (Secant modulus) E_{eqv} is defined as

$$E_{eqv} = \frac{\sigma_{max}{}^{+} - \sigma_{max}{}^{-}}{\varepsilon_{max}{}^{+} - \varepsilon_{max}{}^{-}} \tag{6}$$

The dissipated hysteretic energy ΔW is defined as

$$\Delta W = \int \sigma \mathrm{d}\varepsilon \tag{7}$$

The equivalent damping ratio ξ_{eqv} is calculated as

$$\xi_{eqv} = \frac{\Delta W}{4\pi W_s} \tag{8}$$

where $\varepsilon_{max}{}^{+}$ and $\varepsilon_{max}{}^{-}$ indicate the strains of the maximum amplitude in the positive and negative directions; $\sigma_{max}{}^{+}$ and $\sigma_{max}{}^{-}$ represent the corresponding stresses at $\varepsilon_{max}{}^{+}$ and $\varepsilon_{max}{}^{-}$; ε is the loading displacement for any deformation; σ is the corresponding damping force at ε; W_s denotes the elastic strain energy at maximum deformation.

Mechanical performance indicators revealed significant pre-compression and frequency dependence in the hysteretic behavior of high damping rubber elastomers, as shown in Fig. 8. As pre-compression increased from 3.0 to 7.0 mm, the equivalent modulus escalated by 7.5 %–24.6 %. In addition, energy dissipation surged 10.6 to 11.9 times compared to that at 3.0 mm pre-compression. When frequency increased from 0.1 Hz to 20.0 Hz, both the equivalent modulus and energy dissipation were amplified. Specifically, the equivalent modulus increased by 71.2 %–91.4 %, hysteretic energy grew 3.8 times, and the peak equivalent damping ratio reached 0.169. However, under loading conditions of large pre-compression, wide amplitude, and high frequency (D3.0P7.0F20.0), the equivalent damping ratio decreased by 17.2 %. This reduction was attributed to the enhanced nonlinearity, which caused the hysteresis loop to become more concave and resulted in an increase in strain energy. Moreover, the frequency variations at low range exerted a more pronounced influence on the hysteresis loop and mechanical properties, indicating that the sensitivity of the frequency dependence was inversely proportional to the frequency.

From a microscopic perspective, the frequency-dependent effect can be explained by the response of polymer networks under external force. With increasing loading frequency, the dominant energy dissipation mechanism gradually transitions from conformational adjustments and dynamic hydrogen bond breakage-reformation to segmental motions of polymer chains with filler-matrix interfacial friction. This mechanism leads to significant energy dissipation, thereby imparting the elastomer with excellent vibration damping and energy absorption capabilities. When the loading frequency is high, the mobility of the chain segments becomes increasingly restricted, and interfacial friction between fillers and the matrix is intensified. Meanwhile, molecular conformations and hydrogen bonds have insufficient time to adjust and recombine. As a result, the mechanical behavior tends to a glassy response and exhibits increased stiffness. Consequently, even as the frequency continues to rise, the variations in the mechanical performance indicators remain slight compared to those observed at lower frequencies.

3.3. Results of temperature-controlled dynamic cyclic testing

3.3.1. Temperature dependence

The thermomechanical response of the high damping rubber-based elastomer was investigated through temperature-controlled hysteresis tests, as depicted in Fig. 9.

Two representative conditions, D1.0P3.0 and D3.0P10.0, demonstrated pronounced key temperature effects. Temperature significantly affected the area and shape and area of the hysteresis loop. When the temperature dropped, the hysteresis loops exhibited increased modulus, damping capacity, and nonlinearity—similar to the effects of elevated loading frequency. This observation pointed to a distinct property of polymers, the dependence on temperature and frequency (time), known as the frequency-temperature superposition [54,55]. Increasing

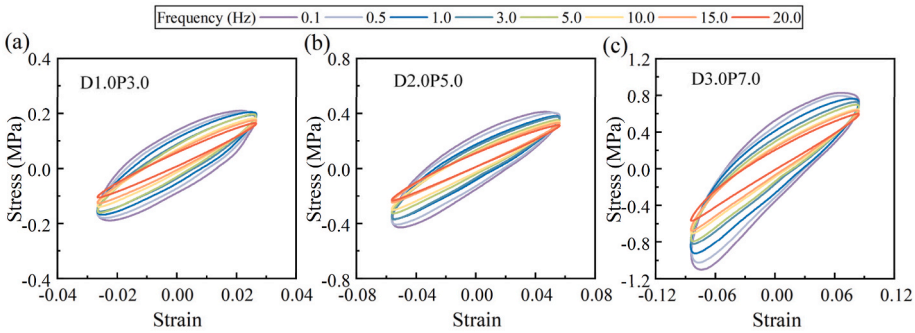

Fig. 7. Stress-strain loops of pre-compressed specimens at 0.1 Hz–20.0 Hz.

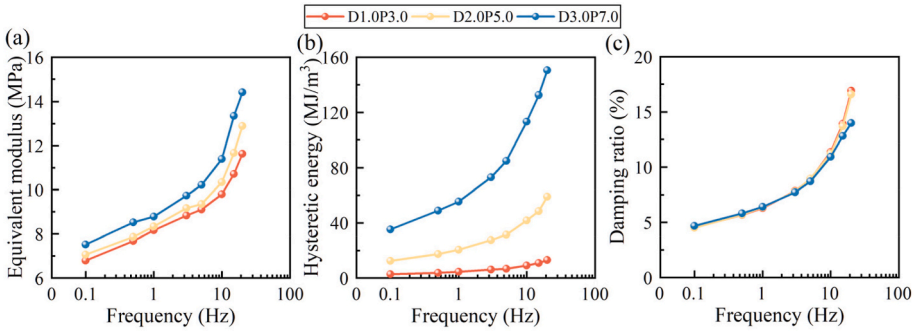

Fig. 8. Variation of mechanical performance indicators with frequency.

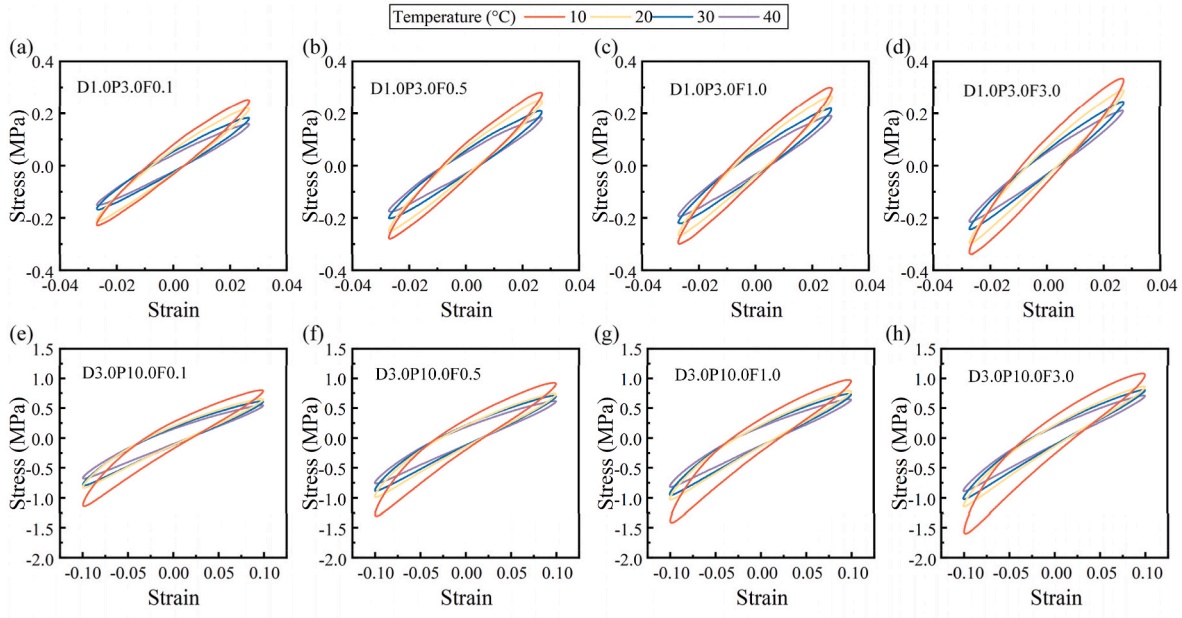

Fig. 9. Stress-strain loops of pre-compressed specimens at 10.0, 20.0, 30.0, and 40.0 °C.

temperature and decreasing frequency have the same effect on the deformation of polymers. An equivalent relation exists between temperature and frequency, describing the synergistic effect on the microstructure of polymers.

To avoid the influence of frequency on hysteresis loops, the temperature dependence on mechanical performance indicators was analyzed at a constant loading frequency of 1.0 Hz. The variations of mechanical performance indicators across different temperature, pre-compression, and amplitude were drawn in Figs. 10–12.

Within the working temperature range of the high damping rubber-based elastomers in seismic applications, temperature exhibited a generally negative correlation with the equivalent modulus, hysteretic energy, and equivalent damping ratio. The mechanical performance in the low-temperature range was significantly enhanced. Specifically, there was a 35.2–38.8 % reduction in equivalent modulus, a 43.1–50.4 % loss in hysteresis energy, and a 15.5–16.3 % drop in damping ratio at 40 °C compared to 10 °C. More noticeable alterations were observed at 20 °C compared to 10 °C, with an 11.2–21.8 % reduction in equivalent modulus, a 24.7–34.2 % loss in hysteresis energy, and a 12.8–13.1 % drop in damping ratio. The temperature dependence on equivalent

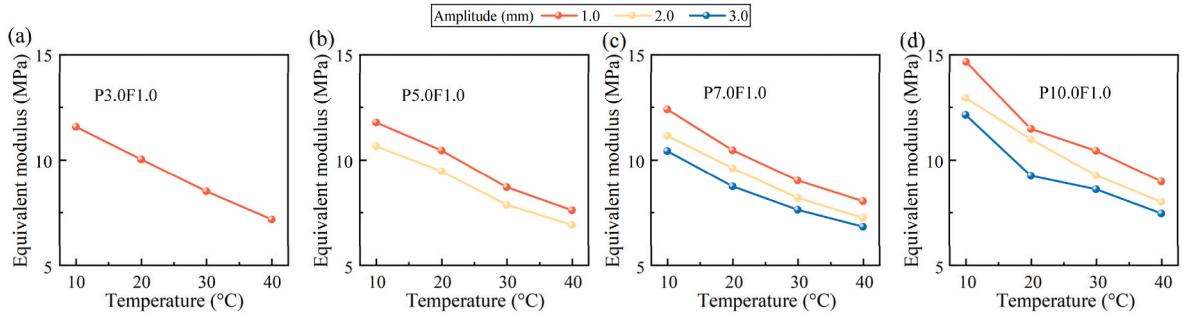

Fig. 10. Variation of equivalent modulus with temperature.

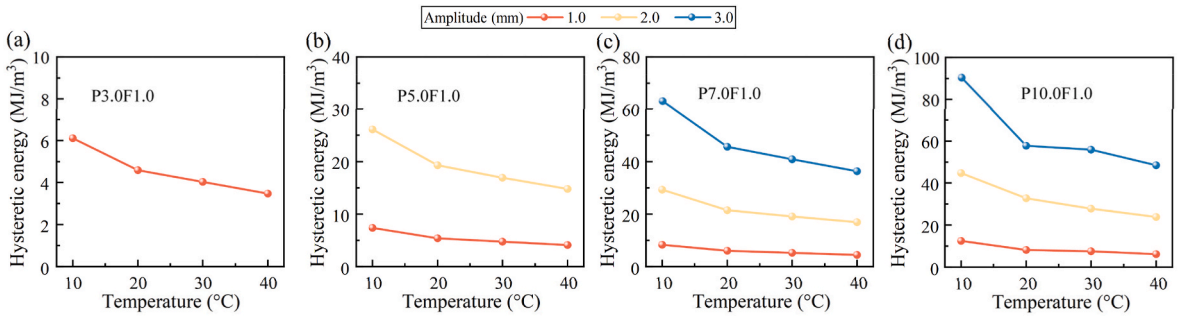

Fig. 11. Variation of hysteretic energy with temperature.

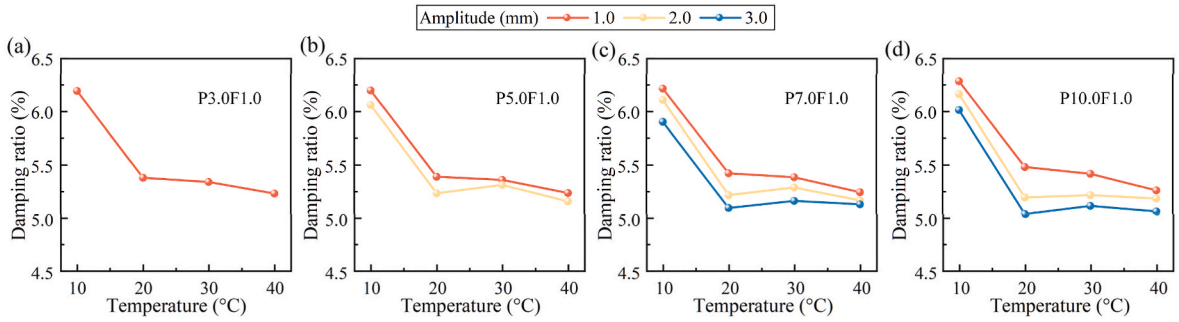

Fig. 12. Variation of equivalent damping ratio with temperature.

modulus was independent of the pre-compression and amplitude. Conversely, the temperature dependence on hysteretic energy displayed amplified sensitivity at larger amplitudes, reflecting nonlinear characteristics. As the temperature increased, the equivalent damping ratio first decreased and then fluctuated slightly, which is attributed to the competing influences between the equivalent modulus and the hysteretic energy.

Temperature greatly influences the macroscopic mechanical performance through modulating the polymer chain mobility, filler-matrix interaction, and dynamic hydrogen bond equilibrium. High temperature enhances the thermal motion of polymer chains, reduce the interfacial adhesion between fillers and matrix, weaken the strength of hydrogen bonds, accelerate bond breaking, and suppress the recombine ability of hydrogen bonds. Chain segments can more readily respond to external forces through sliding or conformational adjustments, fillers are prone to thermal debonding, and hydrogen bond energy is lowered. Consequently, the mechanical performance exhibits reduced energy dissipation efficiency, decreased stiffness, and diminished nonlinear characteristics. In contrast, at low temperatures, chain segment mobility is restricted, filler-matrix interaction is enhanced, and the thermal stability of hydrogen bonds is enhanced. Molecular chain orientation and entanglement are less prone to relaxation. Moreover, hydrogen bonds serve as more stable physical crosslinks that require more energy to break, leading to high stiffness, large hysteretic energy, and strong nonlinearity.

Frequency-temperature superposition can also be explained by considering the microscopic structure of polymers. When the temperature decreases or the loading frequency increases, the viscous flow of polymer chains is restricted. This restriction enhances the internal friction of chain segments, enhances filler-matrix interaction, and improves the dissipated energy from hydrogen bonds, resulting in higher stiffness and greater energy dissipation. Instead, when the temperature increases or the loading frequency decreases, the motion of the chain segments becomes easier and fuller. The interfacial adhesion between fillers and matrix weakens, and the energy absorbed from internal friction and hydrogen bonds gradually declines, with a reduction of stiffness and dissipated energy. This equivalence between temperature and frequency is a manifestation of the frequency-temperature superposition principle and an important characteristic of the dynamic response of polymers on microscopic and macroscopic scales.

3.3.2. *Pre-compression dependence*

To ensure comparability, the strain calculations in this section were normalized using the original specimen height before pre-compression. Fig. 13 illustrates the representative hysteresis curves under varying pre-compression levels of 3.0, 5.0, 7.0, and 10.0 mm (corresponding to pre-strains of 0.075, 0.125, 0.175, and 0.25, respectively). The tests were conducted at a constant amplitude of 1.0 mm (corresponding to 0.025 strain) and a frequency of 1.0 Hz. The pre-compression dependence was quantified through mechanical performance indicators, as shown in Fig. 14. Increasing the pre-strain from 0.075 to 0.25 induced three distinct changes. First, the slope of the hysteresis loops became steeper, with the modulus elevating by 41.2–56.3 %. Second, the area of the hysteresis loops expanded, resulting in a 44.0–65.0 % increase in energy dissipation. Third, the nonlinear behavior became more evident. The improvement in energy dissipation exceeded the enhancement in modulus for higher pre-compression, resulting in a gentle increase in the damping ratio. Besides, a higher level of pre-compression led to more substantial enhancements in the mechanical property indicators. It has been previously verified that the static preloading path followed along the hyperelastic curve when pre-compression is applied to polymers at an extremely low rate. Therefore, pre-compression shifts the initial loading point towards higher strains along the hyperelastic curve. Consequently, subsequent cyclic loading occurs in the region with higher resistance and modulus, as shown in Fig. 6 (a).

Pre-compression induces the polymer network to withstand a high strain state beforehand, where filler aggregates and chain segments are squeezed tighter and denser under compression. This pre-strain state restricts the mobility of both chain segments and filler particles during subsequent cyclic deformation, amplifying internal friction through restricting chain segments slippage and filler-matrix interaction. Simultaneously, pre-compression induces some hydrogen bond rupture,

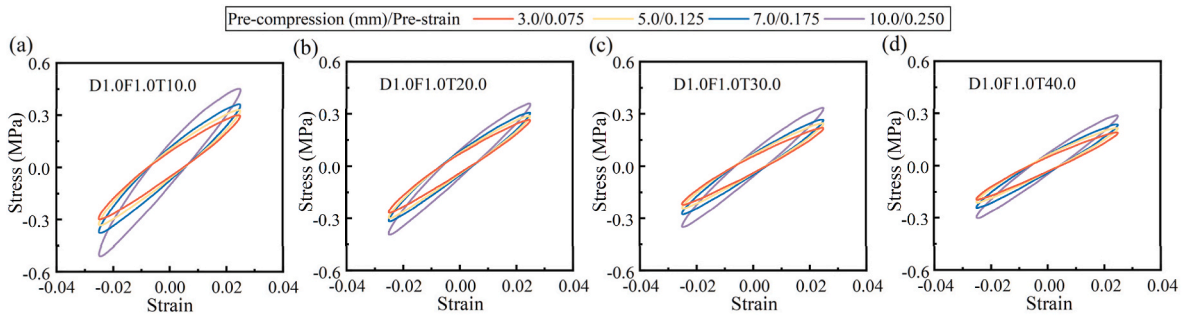

Fig. 13. Stress-strain loops of pre-compressed specimens at 3.0, 5.0, 7.0, and 10.0 mm pre-compression.

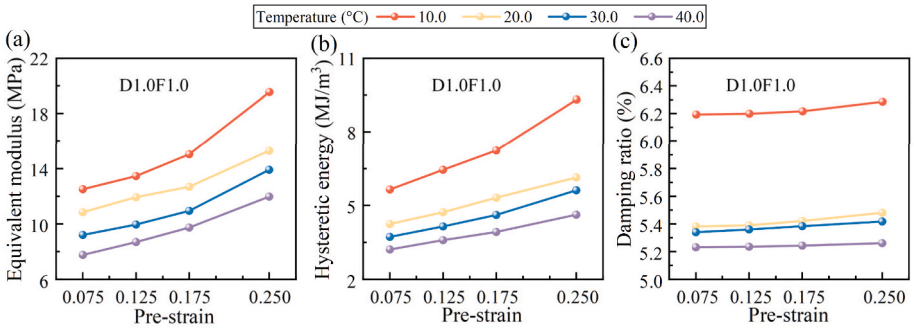

Fig. 14. Variation of mechanical performance indicators with pre-compression.

followed by their reformation at thermodynamically favorable positions, which stabilizes a reinforced transient network with optimized crosslink density. The interplay between restricted molecular mobility and hydrogen bond network reorganization directly manifests macroscopically as elevated stiffness and improved energy dissipation efficiency.

Through the rational design of the preloading process, a higher load-bearing capacity can be achieved while ensuring high energy dissipation and vibration damping performance. This finding is of great significance for vibration damping applications. Pre-compression may provide a more flexible design approach for utilizing the hyperelastic advantages of polymers in vibration damping applications.

3.3.3. *Amplitude dependence*

The amplitude-dependent viscoelastic behavior manifests as a characteristic reduction in dynamic modulus with increasing strain amplitude under cyclic loading, demonstrating the Payne effect. The Payne effect is a hysteretic softening behavior observed under low dynamic strain in filled elastomers [56]. To characterize this phenomenon, cyclic loading tests were conducted at fixed pre-compression (10.0 mm) and frequency (3.0 Hz) with progressively increasing amplitudes (1.0, 2.0, and 3.0 mm). As shown in Fig. 15, hysteresis loops exhibited distinct amplitude-driven modifications. The shape of hysteresis loops became increasingly inflated and buckled as the amplitude increased, although the slope of the loops tended to flatten. The mechanical performance indicators were further calculated to reveal the mechanical trends, as seen in Fig. 16. As the amplitude increased from 1.0 mm to 3.0 mm, the equivalent modulus decreased by 17.5–20.7 %, while the hysteretic energy dissipation significantly increased by 5.8–6.5 times. The equivalent damping ratio initially stabilized before decreasing by 1.2–7.8 %.

The amplitude effect stems from the dynamic competition of among multiscale structural interactions in polymers. Under small displacement amplitudes, the rigid filler network and reversible hydrogen-bonded crosslinks maintain high equivalent stiffness. The filler-matrix interfacial interaction and dynamic hydrogen bond breakage-reformation cycles dominate the energy dissipation mechanism, resulting in a stable damping ratio. However, as the displacement amplitude escalates, the increased molecular chain mobility expands the free volume between chain segments. In addition, the irreversible breakdown of the filled network and the kinetic imbalance between hydrogen bond rupture and recombination collectively induce softening in force. This transition alters the main energy dissipation pathway from reversible interfacial friction and hydrogen bond dynamics to irreversible chain slippage and filler cluster reconfiguration. Consequently, the equivalent

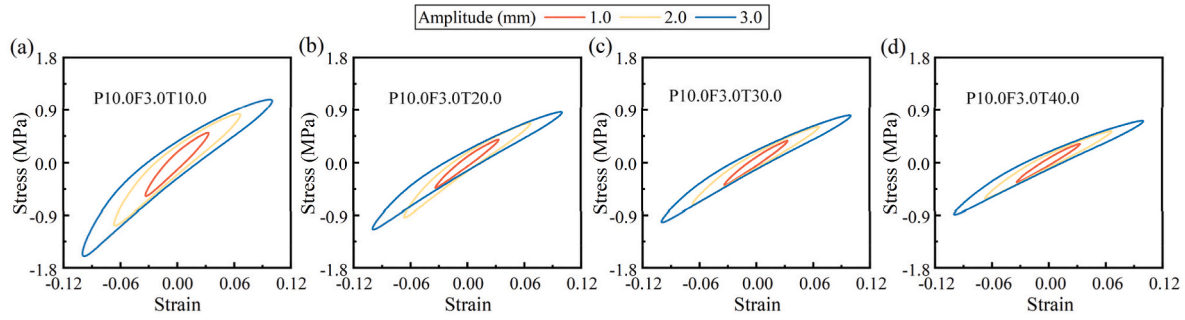

Fig. 15. Stress-strain loops of pre-compressed specimens at 1.0, 2.0, and 3.0 mm amplitude.

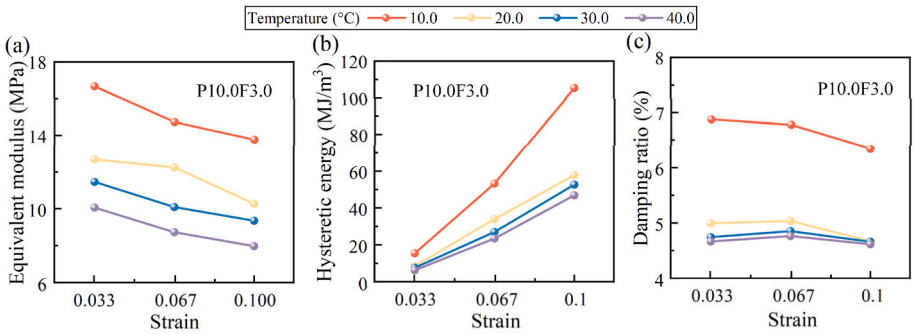

Fig. 16. Variation of mechanical performance indicators with amplitude.

stiffness decreases, accompanied by an expansion of hysteresis loops and a subsequent decline in damping ratio, as evidenced by the amplitude-dependent evolution of mechanical indicators.

4. Conclusions

This study investigated the dynamic mechanical behavior and microscopic energy dissipation mechanisms of pre-compressed high damping rubber-based elastomers. The elastomers were modified with nanofiller reinforcement and sacrificial bonds and evaluated under coupled service conditions, including pre-compression, cyclic loading, and thermal variations. The main findings are summarized below.

(1) Pre-compression shifts the operational region of cyclic loading along the hyperelastic stress-strain curve. This shift significantly enhances stiffness and energy dissipation while reducing the Mullins effect. Pre-strain levels of 7.5 %–25 % amplify equivalent modulus by 41.2–56.3 % and hysteretic energy by 44.0–65.0 %, attributed to restricted chain mobility, enhanced filler-matrix interfacial interaction and hydrogen bond network dynamic reorganization.
(2) The elastomer exhibits high damping performance over the test frequency band of 0.1–20.0 Hz and test temperature range of 10.0–40.0 °C. Increasing frequency elevates the equivalent modulus by 71.2 %–91.4 % and increases hysteretic energy by 3.8 times. In contrast, rising temperature weakens the equivalent modulus by 35.2 %–38.8 % and reduces energy dissipation by 43.1 %–50.4 %. These changes are driven by restricted polymer chain mobility, intensified filler-matrix adhesion, and hydrogen bond dynamics at higher frequencies and lower temperatures. However, excessive frequency of 20.0 Hz under large pre-compression marginally reduces damping ratio due to nonlinear hysteresis loop distortion.
(3) Amplitude increases from 3.3 % to 10 % induce the Payne effect under 25 % pre-strain. This effect reduces the equivalent modulus by 17.5 %–20.7 % and amplifies hysteretic energy dissipation by 5.8–6.5 times. This transition reflects a change of energy dissipation mechanisms from reversible hydrogen bond dynamics to irreversible chain slippage and filler network breakdown.
(4) The combination of chemical crosslinks, nanofiller networks, and dynamic hydrogen bonds establishes a multi-level energy dissipation system. Hydrogen bonds act as reversible sacrificial bonds, while nanofillers restrict chain mobility and enhance interfacial friction. These mechanisms collectively enable high damping performance across wide operational ranges, suitable for pre-loaded damping components in vibration control engineering.
(5) Further studies are planned to elucidate the mechanisms affecting the damping performance by FTIR analysis and molecular dynamics simulations. These studies will focus on the formation and dynamic behavior of hydrogen bonds under various temperature and loading conditions, thus consolidating current findings and helping to develop predicting models for the high damping rubber-based elastomer under pre-compression.

CRediT authorship contribution statement

Jia-Xuan He: Writing – review & editing, Writing – original draft, Visualization, Validation, Investigation, Formal analysis, Data curation. **Zhao-Dong Xu:** Supervision, Project administration, Funding acquisition. **Zhong-Wei Hu:** Writing – review & editing, Investigation. **Teng Ge:** Writing – review & editing. **Qiang-Qiang Li:** Writing – review & editing. **Yao-Rong Dong:** Writing – review & editing. **Gabriele Milani:** Writing – review & editing, Funding acquisition.

Declaration of competing interest

The authors declare that they have no known competing financial interests or personal relationships that could have appeared to influence the work reported in this paper.

Acknowledgments

The authors express their appreciation for the financial support from National Natural Science Foundation of China (52130807), National Program on Key R&D Project of China (2022YFE0210500), Jiangsu Province International Cooperation Project (BZ2022037), and China Scholarship Council (CSC) scholarship program (202206090183).

Gabriele Milani gratefully acknowledges the financial support of the Italian Ministry of Scientific Research MUR within the research project PRIN-2022 (https://www.dabc.polimi.it/en/progetto/advanced-mechanical-models-and-computational-methods-for-large-scale-3d-printing-of-innovative-concrete-structures/) titled “Advanced mechanical models and computational methods for large-scale 3D printing of innovative concrete structures (COMˆ3D CREATE)” (National PI: Prof. Andrea Chiozzi, Local PI: Prof. Gabriele Milani). Finanziato dall’Unione europea- Next Generation EU, Missione 4 Componente 1 CUP D53D23004070006.

Data availability

Data will be made available on request.

References

[1] J.S. Bergström, M.C. Boyce, Large strain time-dependent behavior of filled elastomers, Mech. Mater. 32 (2000) 627–644, https://doi.org/10.1016/S0167-6636(00)00028-4.
[2] M.O. Saed, W. Elmadih, A. Terentjev, D. Chronopoulos, D. Williamson, E. M. Terentjev, Impact damping and vibration attenuation in nematic liquid crystal elastomers, Nat. Commun. 12 (2021) 6676, https://doi.org/10.1038/s41467-021-27012-1.
[3] D. Lin, F. Yang, D. Gong, R. Li, A new vibration isolator integrating tunable stiffness-damping and active driving properties based on radial-chains

magnetorheological elastomer, Mech. Syst. Signal Process. 183 (2023) 109633, https://doi.org/10.1016/j.ymssp.2022.109633.
[4] C. Zhang, X. Gou, R. Xiao, Hysteresis in glass microsphere filled elastomers under cyclic loading, Polym. Test. 95 (2021) 107081, https://doi.org/10.1016/j.polymertesting.2021.107081.
[5] P. Garnier, J.-B. Le Cam, M. Grédiac, The influence of cyclic loading conditions on the viscoelastic properties of filled rubber, Mech. Mater. 56 (2013) 84–94, https://doi.org/10.1016/j.mechmat.2012.10.001.
[6] A.-M.M.R. Persson, E. Andreassen, Cyclic compression testing of three elastomer types—a thermoplastic vulcanizate elastomer, a liquid silicone rubber and two ethylene-propylene-diene rubbers, Polymers 14 (2022) 1316, https://doi.org/10.3390/polym14071316.
[7] A.B. Chai, A. Andriyana, E. Verron, M.R. Johan, Mechanical characteristics of swollen elastomers under cyclic loading, Mater. Des. 44 (2013) 566–572, https://doi.org/10.1016/j.matdes.2012.08.027.
[8] I.M. Alarifi, A comprehensive review on advancements of elastomers for engineering applications, Biodegrad, Polym. Eng. Appl. 6 (2023) 451–464, https://doi.org/10.1016/j.aiepr.2023.05.001.
[9] M.M. Riyadh, S.S. Osman, M.S. Alam, Experimental investigation of novel carbon-fiber reinforced elastomeric isolators with polyurethane cores under vertical and lateral loading, Eng. Struct. 275 (2023) 115186.
[10] S. Somanath, R. Marimuthu, S. Krishnapillai, Frequency domain analysis of pre-stressed elastomeric vibration isolators, Def. Technol. 25 (2023) 33–47, https://doi.org/10.1016/j.dt.2022.10.004.
[11] E. Choi, H. Youn, K. Park, J.-S. Jeon, Vibration tests of precompressed rubber springs and a flag-shaped smart damper, Eng. Struct. 132 (2017) 372–382, https://doi.org/10.1016/j.engstruct.2016.11.050.
[12] J.-X. He, Z.-D. Xu, L.-Y. Zhang, Z.-H. Lin, Z.-W. Hu, Q.-Q. Li, Y.-R. Dong, Shaking table tests and seismic assessment of a full-scale precast concrete sandwich wall panel structure with bolt connections, Eng. Struct. 278 (2023) 115543, https://doi.org/10.1016/j.engstruct.2022.115543.
[13] X. Wang, Z.-D.Xu, J. Dai, H. Peng, Z. Chen, Z. Wang, et al. Flutter behavior of functionally graded graphene origami-reinforced auxetic metamaterial compositelaminated plates in supersonic flow, Eng. Struct. 336 (2025) 120318, doi:10.1016/j.engstruct.2025.120318.
[14] A. Elgammal, A. Seleemah, M. Elsharkawy, H. Elwardany, Comprehensive review on seismic pounding between adjacent buildings and available mitigation measures, Arch. Comput. Methods Eng. 31 (2024) 4269–4304, https://doi.org/10.1007/s11831-024-10114-6.
[15] E. Choi, G. Choi, H.-T. Kim, H. Youn, Smart damper using the combination of magnetic friction and pre-compressed rubber springs, J. Sound Vib. 351 (2015), https://doi.org/10.1016/j.jsv.2015.04.028.
[16] A. Issa, N. Rahgozar, M.S. Alam, Experimental investigation and seismic analysis of a novel self-centering piston-based bracing archetype with polyurethane cores, Eng. Struct. 283 (2023) 115735, https://doi.org/10.1016/j.engstruct.2023.115735.
[17] Y. Zhou, Z. Zhang, Experimental and analytical investigations on compressive behavior of thick rubber bearings for mitigating subway-induced vibration, Eng. Struct. 270 (2022) 114879, https://doi.org/10.1016/j.engstruct.2022.114879.
[18] V. Morovati, A. Bahrololoumi, R. Dargazany, Fatigue-induced stress-softening in cross-linked multi-network elastomers: effect of damage accumulation, Int. J. Plast. 142 (2021) 102993, https://doi.org/10.1016/j.ijplas.2021.102993.
[19] A. Vahidifar, E. Esmizadeh, G. Naderi, A. Varvani-Farahani, Ratcheting response of nylon fiber reinforced natural rubber/styrene butadiene rubber composites under uniaxial stress cycles: experimental studies, Fatig. Fract. Eng. Mater. Struct. 41 (2018) 348–357, https://doi.org/10.1111/ffe.12684.
[20] G. Scetta, J. Ju, N. Selles, P. Heuillet, M. Ciccotti, C. Creton, Strain induced strengthening of soft thermoplastic polyurethanes under cyclic deformation, J. Polym. Sci. 59 (2021) 685–696, https://doi.org/10.1002/pol.20210060.
[21] P. Ortiz-Serna, R. Díaz-Calleja, M. Sanchis, G. Floudas, R. Nunes, A. Martins, L. Visconte, Dynamics of natural rubber as a function of frequency, temperature, and pressure. A dielectric spectroscopy investigation, Macromolecules 43 (2010) 5094–5102, https://doi.org/10.1021/ma1004869.
[22] A. Ansari, T.R. Mohanty, S. Sarkar, S. Ramakrishnan, S. Amarnath, N.K. Singha, Epoxy modified styrene butadiene rubber (SBR) in green tire application, Eur. Polym. J. 213 (2024) 113069, https://doi.org/10.1016/j.eurpolymj.2024.113069.
[23] Y. Han, H. Zheng, Y. Liu, M. Wang, J. Wang, Q. Xie, S. Jing, X. Qin, L. Zhang, Synergistic development of natural rubber/butyl rubber composites for improved interfacial bonding and enhanced shock-absorbing capabilities, ACS Omega 9 (2024) 13897–13905, https://doi.org/10.1021/acsomega.3c08996.
[24] X. Wang, D. Yin, Z. Chen, Y. Hu, S. Hu, X. Zhao, CO2-based polyurethane elastomers with enhanced mechanical and tunable room-temperature damping performances, Eur. Polym. J. 220 (2024) 113499, https://doi.org/10.1016/j.eurpolymj.2024.113499.
[25] B. Yoon, J.Y. Kim, U. Hong, M.K. Oh, M. Kim, S.B. Han, J.-D. Nam, J. Suhr, Dynamic viscoelasticity of silica-filled styrene-butadiene rubber/polybutadiene rubber (SBR/BR) elastomer composites, Compos. Part B Eng. 187 (2020) 107865, https://doi.org/10.1016/j.compositesb.2020.107865.
[26] S. Utrera-Barrios, R. Perera, N. León, M.H. Santana, N. Martínez, Reinforcement of natural rubber using a novel combination of conventional and in situ generated fillers, Composer Part C Open Access 5 (2021) 100133, https://doi.org/10.1016/j.jcomc.2021.100133.
[27] M. Dadkhah, M. Messori, A comprehensive overview of conventional and bio-based fillers for rubber formulations sustainability, Mater. Today Sustain. (2024) 100886, https://doi.org/10.1016/j.mtsust.2024.100886.
[28] M.J. Azizli, M. Mokhtary, H.A. Khonakdar, V. Goodarzi, Compatibilizer/graphene/carboxylated acrylonitrile butadiene rubber (XNBR)/ethylenepropylenediene monomer (EPDM) nanocomposites: morphology, compatibility, rheology and mechanical properties, J. Appl. Polym. Sci. 137 (2020), https://doi.org/10.1002/app.49331 app49331.
[29] M.J. Azizli, Amin Iranpoury, Mohammad Barghamadi, Katayoon Rezaeeparto, Somayeh Parham, Zahra Jahankhah, Masoud M. Mokhtary, Compatibilization Hashemi, Of novel GO-XNBR-g-GMAC/XNBR/XSBR nanocomposites: the relationship between structure and properties, Compos. Interfaces 30 (2023) 803–826, https://doi.org/10.1080/09276440.2023.2179234.
[30] M.J. Azizli, M. Mokhtary, H.A. Khonakdar, V. Goodarzi, Hybrid rubber nanocomposites based on XNBR/EPDM: select the best dispersion type from different nanofillers in the presence of a compatibilizer, J. Inorg. Organomet. Polym. Mater. 30 (2020) 2533–2550, https://doi.org/10.1007/s10904-020-01502-z.
[31] M.J. Azizli, S. Rezaeinia, K. Rezaeeparto, M. Mokhtary, F. Askari, Enhanced compatibility, morphology, rheological and mechanical properties of carboxylated acrylonitrile butadiene rubber/chloroprene rubber/graphene nanocomposites: effect of compatibilizer and graphene content, RSC Adv. 10 (2020) 11777–11790, https://doi.org/10.1039/D0RA00517G.
[32] E. Ducrot, Y. Chen, M. Bulters, R.P. Sijbesma, C. Creton, Toughening elastomers with sacrificial bonds and watching them break, Science 344 (2014) 186–189, https://doi.org/10.1126/science.1248494.
[33] H. Yokochi, R.T. O'Neill, T. Abe, D. Aoki, R. Boulatov, H. Otsuka, Sacrificial mechanical bond is as effective as a sacrificial covalent bond in increasing cross-linked polymer toughness, J. Am. Chem. Soc. 145 (2023) 23794–23801.
[34] C. Gong, C. Xie, H. Zhu, W. Ding, J. Song, Y. Ge, Time-varying compressive properties and constitutive model of EPDM rubber materials for tunnel gasketed joint, Constr. Build. Mater. 433 (2024) 136734, https://doi.org/10.1016/j.conbuildmat.2024.136734.
[35] H. Vatandoost, R. Sedaghati, S. Rakheja, M. Hemmatian, Effect of pre-strain on compression mode properties of magnetorheological elastomers, Polym. Test. 93 (2021) 106888, https://doi.org/10.1016/j.polymertesting.2020.106888.
[36] D. Mistry, N.A. Traugutt, B. Sanborn, R.H. Volpe, L.S. Chatham, R. Zhou, B. Song, K. Yu, K.N. Long, C.M. Yakacki, Soft elasticity optimises dissipation in 3D-printed liquid crystal elastomers, Nat. Commun. 12 (2021) 6677, https://doi.org/10.1038/s41467-021-27013-0.
[37] A.-M.M.R. Persson, E.L. Hinrichsen, E. Andreassen, On the temperature dependence of the cyclic compression behaviour of a thermoplastic vulcanizate elastomer, Polym. Test. 112 (2022) 107650, https://doi.org/10.1016/j.polymertesting.2022.107650.
[38] Q.-Q. Li, Z.-D. Xu, Y.-R. Dong, J.-X. He, Y. Tian, Z.-H. He, Y.-Q. Guo, Mechanical property tests and physics-informed data-driven modeling of viscoelastic materials subjected to thermal-oxidative aging, Constr. Build. Mater. 414 (2024) 134920, https://doi.org/10.1016/j.conbuildmat.2024.134920.
[39] Y. Xu, Z.-D. Xu, H. Hu, Y.-Q. Guo, X.-H. Huang, Z.-W. Zhang, T. Zhang, C. Xu, Experiment, simulation, and theoretical investigation of a new type of interlayer connections enhanced viscoelastic damper, Int. J. Struct. Stabil. Dynam. (2024) 2550045, https://doi.org/10.1142/S0219455425500452.
[40] Y. Xu, Z.-D. Xu, Y.-Q. Guo, W. Sarwar, W. She, Z.-F. Geng, Study on viscoelastic materials at micro scale pondering supramolecular interaction impacts with DMA tests and fractional derivative modeling, J. Appl. Polym. Sci. 140 (2023) e53660, https://doi.org/10.1002/app.53660.
[41] T. Ge, X.-H. Huang, Y.-Q. Guo, Z.-F. He, Z.-W. Hu, Investigation of mechanical and damping performances of cylindrical viscoelastic dampers in wide frequency range, Actuators 10 (2021) 71, https://doi.org/10.3390/act10040071.
[42] J.-X. He, Z.-D. Xu, Q.-Q. Li, Z.-W. Hu, Y.-X. Wei, T. Ge, Y.-R. Dong, X.-H. Huang, G. Milani, A time-domain viscoelastic model of nonlinear compression behavior under cyclic loading, Int. J. Eng. Sci. 208 (2025) 104200, https://doi.org/10.1016/j.ijengsci.2024.104200.
[43] T. Ge, Z.-D. Xu, F.-G. Yuan, Development of viscoelastic damper based on NBR and organic small-molecule composites, J. Mater. Civ. Eng. 34 (2022) 04022192, https://doi.org/10.1061/(ASCE)MT.1943-5533.0004339.
[44] S. Kohjiya, A. Kato, Y. Ikeda, Reinforcement of rubber, Springer Ser. Polym. Compos. Mater. (2020).
[45] Y. Hou, Y. Peng, P. Li, Q. Wu, J. Zhang, W. Li, G. Zhou, J. Wu, Bioinspired design of high vibration-damping supramolecular elastomers based on multiple energy-dissipation mechanisms, ACS Appl. Mater. Interfaces 14 (2022) 35097–35104, https://doi.org/10.1021/acsami.2c07604.
[46] J. Xiaolin, X. Min, W. Minhui, M. Yuanhao, Z. Wencong, Z. Yanan, R. Haoxiang, L. Xun, Preparation and molecular dynamics study of polyurethane damping elastomer containing dynamic disulfide bond and multiple hydrogen bond, Eur. Polym. J. 162 (2022) 110893, https://doi.org/10.1016/j.eurpolymj.2021.110893.
[47] G. Pianese, G. Milani, F. Milani, Prediction of the optimal vulcanization of a fiber-reinforced elastomeric isolator made of natural rubber-ethylene propylene diene monomer blend, Polym. Eng. Sci. 63 (2023) 2421–2443, doi:10.1002/pen.26386..
[48] G. Pianese, G. Milani, F. Milani, Kinetic mathematical model with induction and reversion for the vulcanization of natural rubber and ethylene propylene diene monomer blend, Polym. Test. 131 (2024) 108339, https://doi.org/10.1016/j.polymertesting.2024.108339.
[49] A.B. Habieb, F. Milani, G. Milani, G. Pianese, D. Torrini, Vulcanization degree influence on the mechanical properties of Fiber Reinforced Elastomeric Isolators made with reactivated EPDM, Polym. Test. 108 (2022) 107496, https://doi.org/10.1016/j.polymertesting.2022.107496.

[50] L. Luo, F. Zhang, L. Wang, Y. Liu, J. Leng, Recent advances in shape memory polymers: multifunctional materials, multiscale structures, and applications, Adv. Funct. Mater. 34 (2024) 2312036, https://doi.org/10.1002/adfm.202312036.
[51] Q.-Y. Li, Z.-F. Yao, J.-Y. Wang, J. Pei, Multi-level aggregation of conjugated small molecules and polymers: from morphology control to physical insights, Rep. Prog. Phys. 84 (2021) 076601, https://doi.org/10.1088/1361-6633/abfaad.
[52] H.E.H. Meijer, L.E. Govaert, Mechanical performance of polymer systems: the relation between structure and properties, Prog. Polym. Sci. 30 (2005) 915–938, https://doi.org/10.1016/j.progpolymsci.2005.06.009.
[53] J. Diani, B. Fayolle, P. Gilormini, A review on the Mullins effect, Eur. Polym. J. 45 (2009) 601–612, https://doi.org/10.1016/j.eurpolymj.2008.11.017.
[54] D. Jones, On temperature-frequency analysis of polymer dynamic mechanical behaviour, J. Sound Vib. 140 (1990) 85–102.
[55] S. Ronan, T. Alshuth, S. Jerrams, N. Murphy, Long-term stress relaxation prediction for elastomers using the time–temperature superposition method, Mater. Des. 28 (2007) 1513–1523, https://doi.org/10.1016/j.matdes.2006.03.009.
[56] A.R. Payne, The dynamic properties of carbon black-loaded natural rubber vulcanizates. Part I, J. Appl. Polym. Sci. 6 (1962) 57–63, https://doi.org/10.1002/app.1962.070061906.
[57] J.-X. He, Z.-D. Xu, Z.-W. Hu, L.-Y. Zhang, Q.-Q. Li, Y.-R. Dong, G. Milani, A novel multi-dimensional viscoelastic mitigation device: Shake table tests and numerical assessment of precast concrete sandwich wall panel structure, Eng. Struct. 336 (2025) 120388, https://doi.org/10.1016/j.engstruct.2025.120388.
[58] H. Zhang, D. Yu, G. Li, Z. Dong, A feature selection framework of ground motion intensity measure in rapid seismic damage prediction of structures based on ensemble learning, ASCE-J. Struct. Eng. (2025), https://doi.org/10.1061/JSENDH/STENG-13993.